Chalcogenide Letters Vol. 20, No. 10, October 2023, p. 709 - 724

Study of structural, morphological and optical properties of Mn^{+2} doped CdS nanoparticles synthesized at various doping concentration

R. Ranjan[a,b], C. M. S. Negi[b], S. K. Choubey[a], K. P. Tiwary[c,*]
[a]*Department of Electronics and Communication Engineering, Birla Institute of Technology Mesra, Patna Campus, Patna-800014, India*
[b]*Department of Physical Sciences, Banasthali Vidyapith-304022 (Rajasthan), India*
[c]*Department of Physics, Birla Institute of Technology Mesra, Patna Campus, Patna-800014, India*

Manganese-doped cadmium sulphide semiconductor nanoparticles (CdS: Mn) NPs have been created utilizing a microwave-assisted solvothermal technique at different Mn concentrations (0, 1%, 3%, and 5%). The chemicals utilized for the preparation of Mn-doped CdS nanoparticles were sodium sulphide ($Na_2S.xH2O$), manganese chloride ($MnCl_2.4H_2O$), and cadmium acetate ($(CH_3COO)_2Cd._2H_2O$). To determine the structural dimensions of the generated nanoparticles, the Debye-Scherer equation was used to calculate the average crystallite size at the full-width half maximum (FWHM) of the diffraction peaks. FTIR spectra analysis was used to look at the various functional and vibrational groups present in the Mn-doped CdS nanoparticle sample. The structure features of the produced nanoparticles have been examined using X-ray diffraction patterns. Energy dispersive X-rays were employed to ascertain the chemical composition of the synthesized nanoparticles. The optical properties and quantification of the energy band gap of the nanoparticles have been done using UV-V spectroscopy. According to XRD calculations, the cubic zinc-blend structure of the generated NPs had a crystal size of between 4 and 7 nm. By using EDX spectroscopy, the incorporation of Mn at the CdS lattice was confirmed.

(Received July 5, 2023; Accepted October 4, 2023)

Keywords: Mn-doped CdS nanoparticles, X-ray diffraction, FTIR spectra, UV visible spectra

1. Introduction

The direct band gap of cadmium sulphide (CdS), a semiconductor with good optical absorption properties in the visible light spectrum, is 2.42 eV at room temperature. This has led to the application of cadmium sulphide in several photonic devices, such as photovoltaic, photodetectors, lasers, and light-emitting diodes [1–3]. As a result, cadmium sulphide is altered to suit the application's requirements. There has been substantial growth in the utilization of II-VI compound semiconductor nanoparticles in recent times in a variety of fields, including sensors, petrochemical industries, environmental clean-up, agriculture, biochemical applications, purification/water distillation, electronics, medical field, and electrochemical industries [4–7]. Semiconductor materials have a wide variety of applications due to their different structural, optical, electro-catalytic, chemical, and physical capabilities, which are brought on by their unique size, space, and structure [8,9]. Cadmium sulphide (CdS), one of the most well-known compound semiconductors, has found extensive use in a variety of notable fields, including bio-sensing, bio-imaging methods, photovoltaic cells, nano-medicines, molecular pathology, drug delivery, and bio-molecular detection. These applications are all due to CdS's wide band gap, high photosensitivity, and photoconductivity [10-13]. The most common dilute magnetic semiconductors (DMS) are II-VI quantum dot semiconductors (CdSe, ZnS, CdS, etc.) with their

* Corresponding author: kptiwary@bitmesra.ac.in
https://doi.org/10.15251/CL.2023.2010.709

host cations substituted with other elements (such as Cr, Co, Mn, and Fe). The peculiar characteristics of these particles are a result of the interaction between the spin-induced magnetic moments of the transition metal ions and the host semiconductor lattice. [16-21]. To prepare the Mn-doped CdS-sensitive solution, the precursors for manganese and cadmium sulphide were precisely blended. The effect of the dopants on the Mn-doped CdS solution was analyzed. By using a microwave-assisted technique, CdS and other II-VI semiconductor nanoparticles have been synthesized for a variety of applications. The effects of Mn doping on structural, morphological, optical, and magnetic properties are investigated [22-25]. The unique chemical and electronic characteristics of semiconductor quantum dots having a diameter of a few nanometers, suggest their potential application in nonlinear optics, luminescence, electronics, and optoelectronics, among other disciplines [26].

2. Experimental

2.1. Materials

All dilutions and sample preparation were done with distilled water. The chemical reagents employed for the synthesis procedure were of analytical quality and weren't further purified before usage. As precursors, Merck-sourced cadmium acetate $(CH_3COO)_2Cd$, H_2O, manganese chloride ($MnCl_2.4H_2O$), and sodium sulphide ($Na_2S.xH_2O$) were utilized. To remove contaminants, the glassware was acid rinsed and dried which was used for the experiment.

2.2. Synthesis of pure and Mn-doped CdS nanoparticles

Pure and Mn-doped CdS nanoparticles were synthesized using microwave assistance during solvothermal synthesis in an aqueous solution. Pure CdS nanoparticles were synthesized by taking the aqueous solution of cadmium acetate mixed with the aqueous solution of Na_2S in stoichiometric proportion and stirring on a magnetic stirrer at 600 rpm for 5 minutes. Using a magnetic stirrer, the stoichiometric aqueous solutions of manganese chloride ($MnCl_2.4H_2O$) and cadmium acetate $(CH3COO)_2Cd$, H_2O) were mixed. The appropriate schematic diagram of CdS nanoparticles is shown in Fig. 1. The previously combined solution was gradually mixed with sodium sulphide aqueous solution [$Na_2S.2H_2O$] drop by drop, and then the microwave-assisted solvothermal technique started for one complete cycle, consisting of 20 seconds of radiation and 60 seconds of repose. The duty cycle for the microwave process was taken to be 25%.

$$D= t_1/ (t_1+t_2) \text{ --------- } (1)$$

where t_1 = 20 sec (microwave time)

t_2 = 60 sec (relaxation time)

The resulting yellowish colloidal solution was obtained after 15 cycles. After filtering the precipitation, the Mn+2 doped CdS nanoparticles were separated from it and then kept in oven for drying process for 20 hours at 90 degrees Celsius.

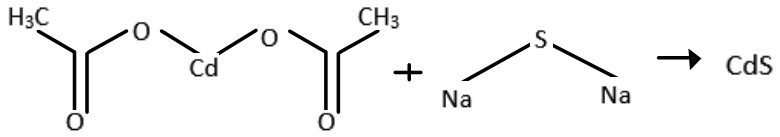

Fig. 1. Synthesis of CdS nanoparticles.

2.3. Characterization technique

The following techniques have been used for characterization:

(a) X-ray Diffraction (XRD): For this technique, the sample's X-ray diffraction patterns were recorded using Cu-K_α radiation with a wavelength of 1.5418 nm. It was possible to determine

the crystallite size of the nanocrystals using the Debye-Scherrer formula and the FWHM of the XRD peaks.

(b) Scanning Electron Microscopy (SEM): A JEOL- JSM-6390LV SEM was utilized to examine the morphology of nanoparticles.

(c) Fourier Transform Infrared Spectroscopy (FTIR): A SHIMADZU-IR PRESTIGE 21 type of equipment was used to collect FTIR data for the purpose of identifying various functional groups.

(d) UV-visible spectroscopy: Optical absorption measurements were made using a RAYLEIGH UV 2601 spectrophotometer in the UV-visible range (300-800 nm).

(e) TRANSMISSION ELECTRON MICROSCOPE (TEM**) -** TEM images are formed **(**Model: JEM-2100) using electrons transmitted through ultra-thin sections, thin film, or powder. The achievable magnification of the TEM can be from 50X to 1,500,000X and a resolution of 0.19 nm depending upon accelerating voltage.

3. Result and discussion

3.1. A. X-RAY Diffraction (XRD)

The structural features of Mn-doped CdS nanoparticles have been investigated using XRD analysis. The XRD patterns showed a significant peak shift because Mn^{2+} ions were absorbed in the substrate CdS lattice. [27] It is typically utilized for phase identification and can also provide a unit cell dimension. The three major peaks of the Mn-doped CdS nanoparticle spectra, shown in Figure 2(a), were identified at 2θ equals for pure CdS (26.52°, 44.16°, and 52.32°), for 1% (26.54°, 44.1°, and 51.64), for 3% (26.56°, 44.1°, and 51.92), and for 5% (26.52°, 44.04°, and 52.042), which correspond to the (111), (220), and (311) planes of the cubic phase of CdS [27]. Due to variations in the concentration of Mn with CdS, angle 2θ has shifted slightly [28]. Moreover, it is observed that with the increase in the doping concentration of Mn, the average crystal size decreases [29] as shown in Table 1. The Debye-Scherer equation determines the average crystallite size at the full-width half maximum (FWHM) from the diffraction peaks of XRD spectra.

$$D = k\lambda / \beta \cos\theta \quad (2)$$

where k is the particle shape factor (taken 0.9), λ is X-ray wavelength (1.5418 Å), β is the FWHM value and θ is the angle of diffraction. The average crystallite size was found to be reduced with the increase in the concentration of Mn-doped in CdS nanoparticles.

The interplanar spacing d can be calculated using Bragg's law as given in equation (3)

$$n\lambda = 2 d \sin\theta \quad (3)$$

where n is the order of diffraction, is the X-ray wavelength (1.5418 Å), d is the inter planer spacing and θ is the angle of diffraction. The value of a can be calculated by using equation (4)

$$d = a / (h^2+k^2+l^2)^{1/2} \quad (4)$$

The other important structural parameter is calculated via the following equations:

$$\text{Volume, } V = a^3 \quad (5)$$

$$\text{Micro strain, } \varepsilon = \beta \cos\theta / 4 \quad (6)$$

$$\text{Dislocation density} = 1/D^2 \quad (7)$$

$$\text{Stacking Fault, } SF = [\, 2\pi 2 /45\sqrt{}\, (3 \tan\theta)] * \beta \quad (8)$$

The structural attributes of Mn-doped CdS nanoparticles, including Inter-planar spacing, full width at half maximum, lattice constant, macro strain, crystallite size, and dislocation density, Stacking Fault, are reported in Table 1. Fig. 2(b) shows that the crystallite size decreases and microstrain increases with increasing Mn concentration in CdS nanoparticles.

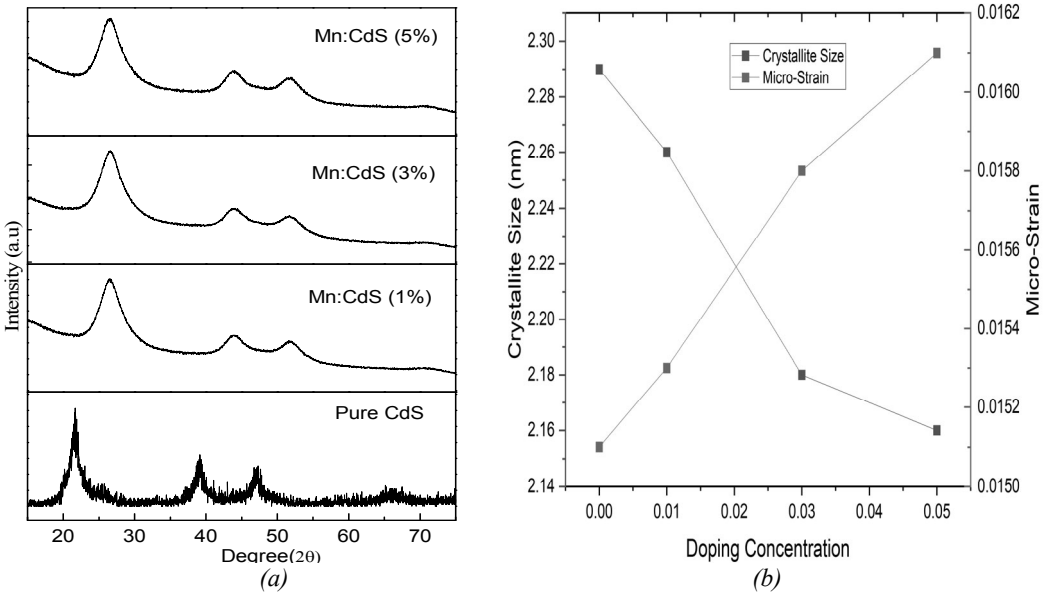

Fig. 2. (a)XRD for Mn-doped CdS NPs (b)plot of Crystallite size and micro strain with doping concentration.

Table 1. Different parameters (Interplanar spacing, lattice constant, volume, micro strain, dislocation density, Average crystallite size) of Mn-doped CdS nanoparticles.

Compound	(2θ) theta (deg)	FWHM (degree)	Interplanar Spacing 'd' (Å)	Lattice Constant 'a' (Å)	Volume of unit cell $(a)^3$ ($Å^3$)	Micro-Strain	Dislocation Density (nm^{-2})	Stacking Fault, (SF)	Average Crystallite Size, D(nm)
Pure CdS	26.52	3.8571	2.3867	5.8469	199.883	0.0151	0.193	0.027	2.29
	44.16	3.4434							
	52.32	3.8947							
CdS: Mn doped (1%)	26.54	3.8693	2.3939	5.8315	198.308	0.0153	0.197	0.027	2.26
	44.1	3.4955							
	51.64	3.9458							
CdS: Mn doped (3%)	26.56	3.898	2.3914	5.8215	197.289	0.0158	0.211	0.028	2.18
	44.1	3.6435							
	51.92	4.1779							
CdS: Mn doped (5%)	26.52	3.903	2.3901	5.8202	197.157	0.0161	0.214	0.027	2.16
	44.04	3.894							
	52.04	4.0292							

3.2. B. Williamson-Hall Method (W-H)

The W-H approach was employed to examine changes in particle size and lattice strain. When it comes to temperature, the expansion brought on by the volume under stress as a result is

reconstructed by displaying the peak. While the strain varies because of the crystal's size, the breadth of the peak generated by the crystals varies by 1/cosθ. The W-H method confirmed the difference that stress produced. The change in behavior as a function of crystal size confirms the distinction between the impacts of crystal size and stress on peak expansion. The Williamsons-Hall method, which incorporates the stress impact of XRD peak expansion and can be used to compute the intrinsic strain and particle size, is very effective and simple. The physical line states that the nanocrystal's small size and stress cause the X-ray diffraction peak expansion, and the total expansion can be expressed as the overall strain size. The size relates to the curvature of the XRD peak's physical line. Hence, the volume stress and overall stress at a specific peak with a hkl value can be stated as

$$\beta = (\beta)_{size} + (\beta)_{strain} \quad (9)$$

The peak width of instrumentally corrected widening at half its highest intensity is known as hkl. The strain-induced peak broadening can be expressed as

$$\beta = k\,\lambda / (D * \text{Cos}\,\theta) + 4\text{Ɛ}\tan\theta \quad (10)$$

Considering that the strain and particle size contributions to the line's broadening are separate from one another. The line's observed broadening is the result of adding equations (9) and (10) are given as follows.

$$\beta\,\text{Cos}\,\theta = k\,\lambda/D + 4\text{Ɛ}\,\text{Sin}\,\theta \quad (11)$$

The preceding equation is converted to a straight-line equation, which is shown in Fig. 3 where it is plotted against 4Sinθ (X-axis) Vs βCosθ (Y-axis) for the compound. The internal strain value is determined by the slope of the straight line. The average crystal size of the compound is determined by the intersection [30, 31].

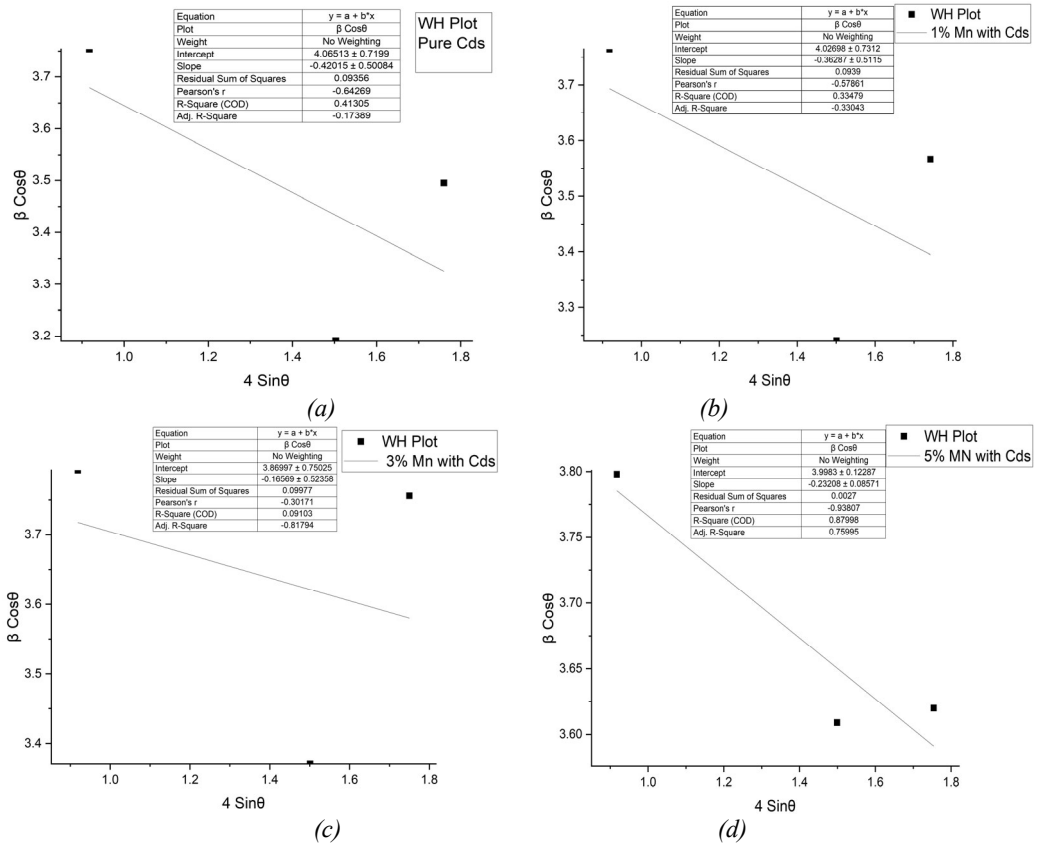

Fig. 3. Williamson-Hall plot (a) Pure CdS (b)1% Mn with CdS (c) 3% Mn with CdS (d)5% Mn with CdS.

3.3. C. Size-strain plot method (SSP)

The contribution of the macrostrain results in the uniformity of the diffracting domains. Size-strain parameters can be extracted using the "size-strain plot" (SSP). The plot is beneficial as less emphasis is placed on information from high-angle reflections. To help with this estimation, it is assumed that the "crystallite size" and the "strain profile" are each represented by a Lorentzian function.

$$(d\ \beta\ \mathrm{Cos}\ \theta\ )^2 = k/D^*((d)^2\ \beta\ \mathrm{Cos}\ \theta) + (\varepsilon / 2)^2 \quad (12)$$

where k is a constant and the form of the particles is specified as 3/4 for spherical particles. Fig. 4 shows the values of $d^2\ \beta\ C\mathrm{os}\ \theta$ and $(d\beta\ C\mathrm{os}\ \theta)^2$ were taken on the x-axis and y-axis respectively for all peaks. By taking the root of the y-intercept, the strain may be determined from the slope linearly fitted data.

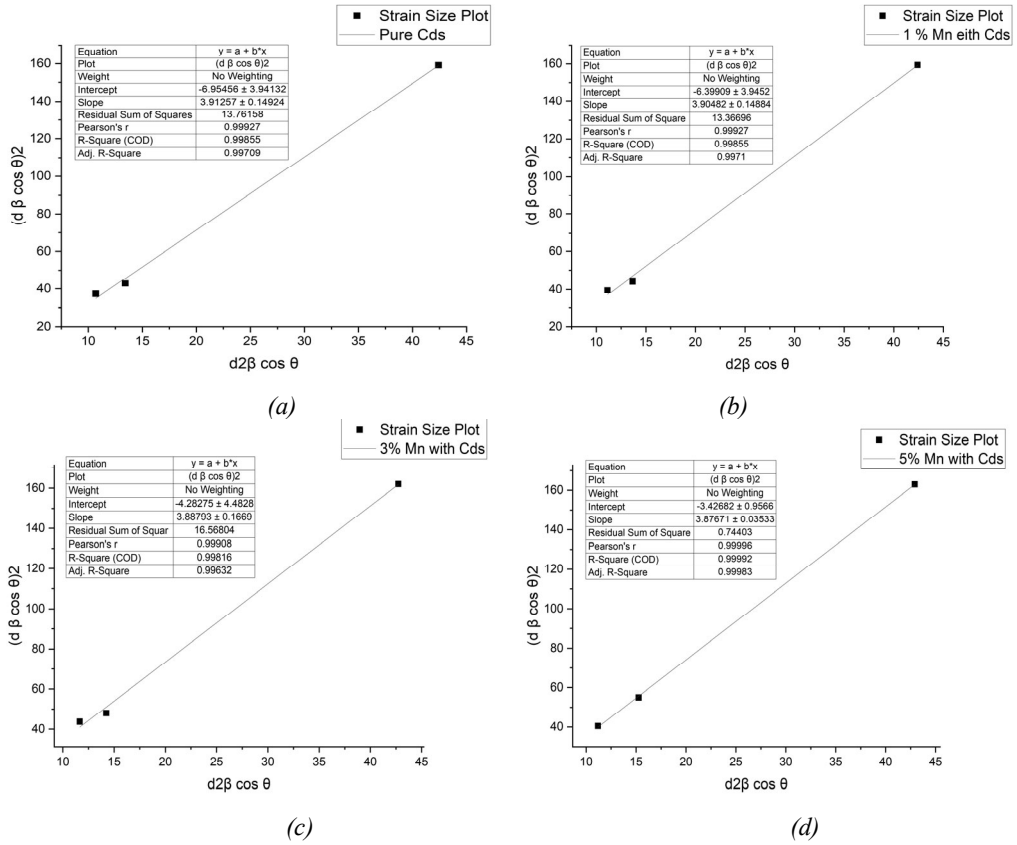

Fig. 4. Size-strain plot(a) Pure CdS (b)1% Mn with CdS (c) 3% Mn with CdS (d)5% Mn with CdS

3.4. D. Halder and Wagner (HW)

Halder and Wagner [10, 11] proposed an alternate equation for determining D and that included the integral breadth, of the reciprocal lattice point and the lattice plane spacing d, for the reciprocal cell:

$$(\beta\ \mathrm{Cos}\ \theta\ /\ \mathrm{Sin}\ (\theta))^2 = k\ \lambda\ /\ D\ (\beta\ \mathrm{Cos}\ \theta\ /\ \mathrm{Sin}^2\ (\theta)) + 16\ \varepsilon^2 \quad (13)$$

The Halder-Wagner (HW) graph as shown in fig. 5 compares $y = (\beta/\ \tan\ \theta)^2$ with $x = \beta/(\tan\theta.\mathrm{Sin}\theta)$. Then, the resulting straight line's slope and y-intercept provide K/D and 16 ε^2 respectively. The value of $K = 4/3$ is believed to be valid on the definition of the crystallite size as the volume-weighted average one for spherical crystallites. Withstanding the approximations and

assumptions used in the development of Eq.13 the HW plot has the huge advantage that data for reflections at low and intermediate diffraction angles are given more weight than those at higher diffraction angles, which are often less accurate.

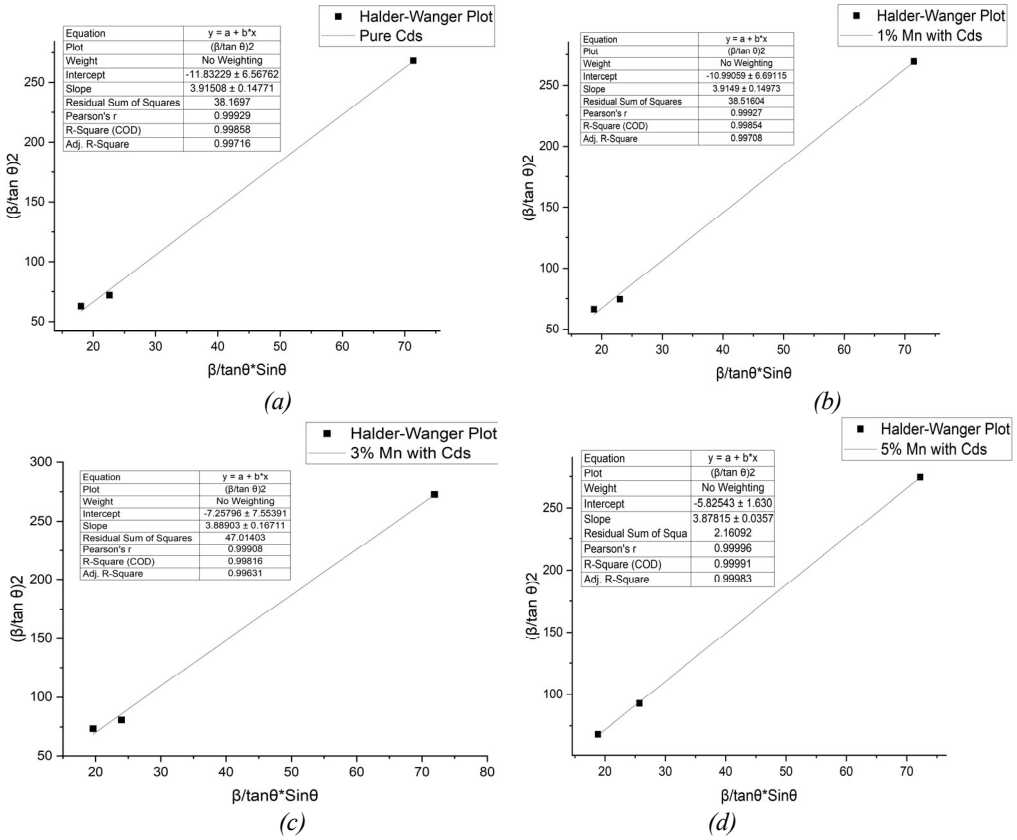

Fig. 5. Halder-Wagner Plot(a) Pure CdS (b)1% Mn with CdS (c) 3% Mn with CdS (d)5% Mn with CdS

3.5. SEM Analysis

The Mn-doped CdS nanoparticles were characterized by SEM using the JEOL Model JSM-6390LV. Fig. 6a, 6b, 6c, and 3d, which show SEM images of the particles, illustrate the surface morphology of the nanoparticles.

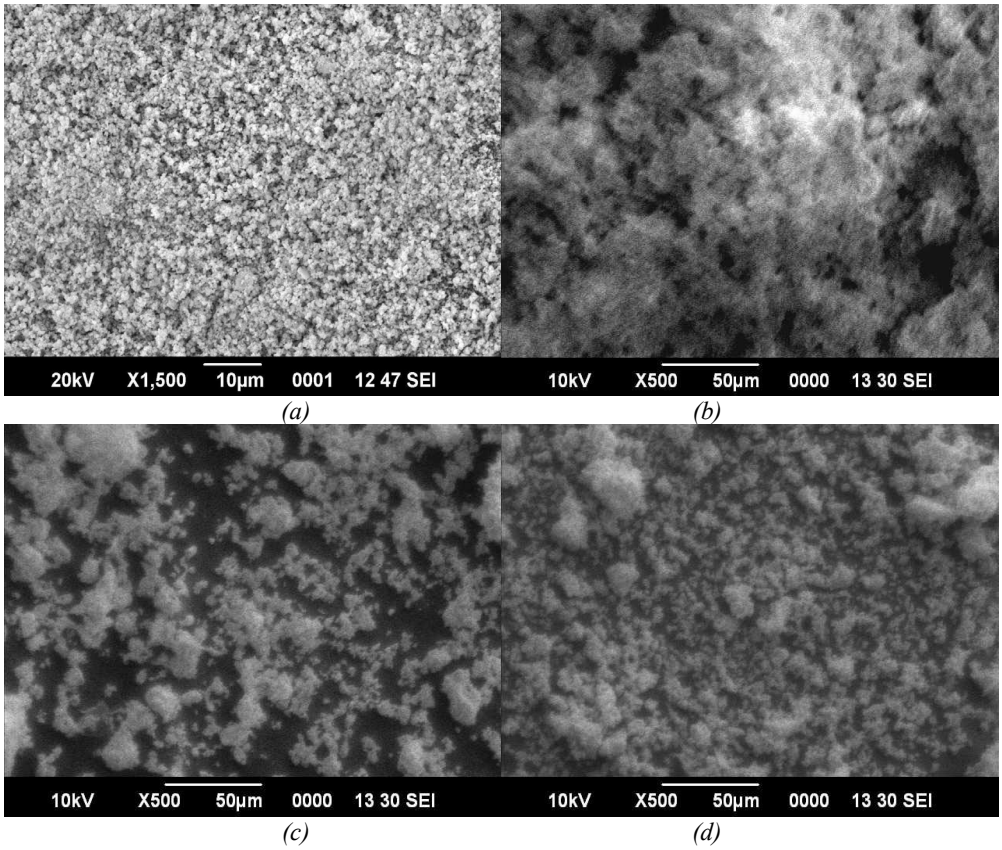

Fig. 6 SEM image of Mn-doped CdS
(a) Pure CdS (b) 1% Mn with CdS (c) 3% Mn with CdS (d)5% Mn with CdS

The SEM micrographs make it clear that nanoclusters have developed. When the Mn doping concentration increases, the physical shape of the individual particles appears to be more spherical than agglomerated. [32]. The micrographs clearly demonstrate that the synthesized nanocrystals have a smooth surface that appears spherical. Using a scanning electron microscope (SEM), the surface morphology of the pure CdS and Mn-doped CdS (pure, 1%, 3%, and 5%) nanoparticles was observed (SEM).In SEM images, it was demonstrated that the shape of the Mn-doped CdS changed as the concentration changed. Figure 6 shows a change in the material particles.

3.6. FTIR Spectroscopy

The different functional and vibrational groups present in the sample of pure and Mn-doped CdS nanoparticles as they were produced have been identified using the FTIR Spectra taken from 400 cm^{-1} to 4000 cm^{-1} at room temperature.

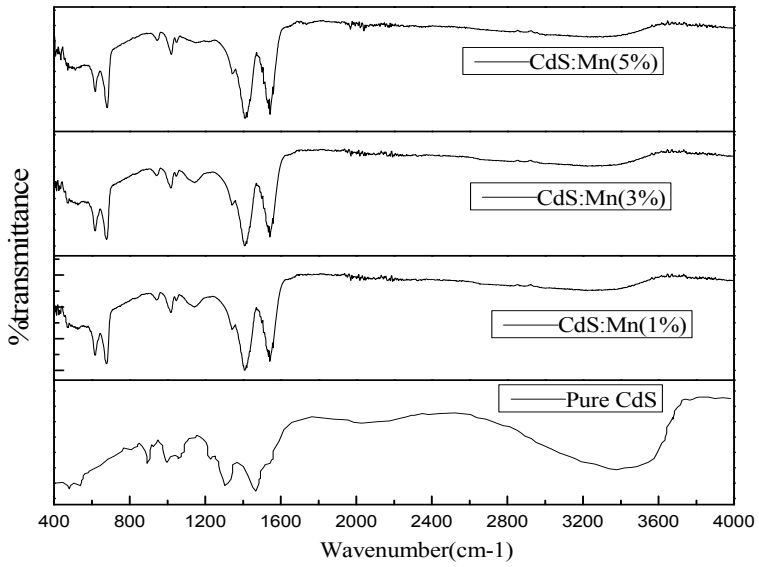

Fig. 7. FTIR of 0, 1%,3%,5% Mn-doped CdS.

Fig. 7 shows the FTIR spectra of pure and Mn (1%,3%,5%) doped CdS nanoparticles. The presence of moisture in the produced sample and the presence of OH stretching vibrations of water molecules are responsible for the weak absorption band between 3400 and 3600 cm^{-1}. The absorption peak between 2800 and 2900 cm^{-1} is responsible for C-H stretching. The moderate and weak signal at 1550 cm^{-1} is explained by the existence of H-O-H bending vibrations in water molecules. The possible explanation of the medium-strong band orientation in the range of 1000–1150 cm^{-1} may be caused by the sulphate group's stretching vibration.

3.7. UV-visible spectroscopy

The optical properties of the synthesized sample were examined using a room-temperature UV-visible spectrophotometer with a 200 nm to 800 nm wavelength range. Fig. 8 shows the optical absorption spectra and band gap estimate of Mn (0%, 1%,3%,5%) doped CdS nanoparticles. The Tauc equation was utilized to calculate the optical bandgap of the generated nanoparticles.

Where is the absorbance, E_g is the band-gap value, h is the energy of the incident photon, A is a constant, and n is assumed to be 1/2 for direct bandgap, the equation is:

$$\alpha h\nu = A (h\nu - E_g)^n \text{ ---------- (14)}$$

The absorption coefficient (α) is estimated by the equation given below:

$$\lambda \alpha = 4 \pi k \text{ ---------- (15)}$$

The bandgap is calculated by extrapolating the graph of $(\alpha h\nu)^2$ versus as shown in Fig.8.

By extrapolating the straight line to the X-axis, the band gap value is determined (in eV). The optical band gap of Mn (0%,1%, 3%, and 5%) doped CdS is determined to be, respectively (2.74eV, 2.88eV, 2.9eV,3.12 eV). The optical band gap of Mn-doped CdS nanoparticles is clearly greater than that of bulk CdS [33, 34]. The band gap is found to increase from undoped to (1%, 3%, and 5%) Mn-doped. This is due to the quantum size effect of nanoparticles. The resulting band gap values coincide with the fact that the band gap increases as crystallite size decreases.

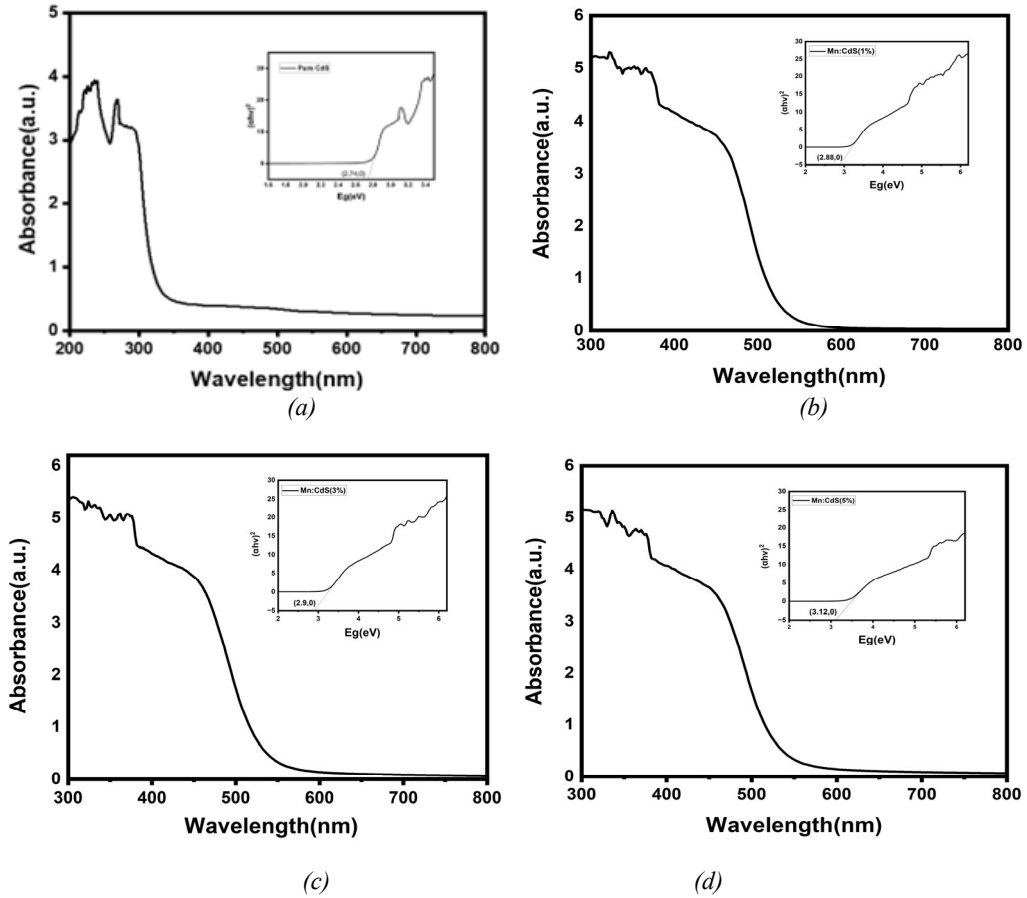

Fig. 8. Absorption spectra and energy bandgap of (i) pure CdS (ii)1%, Mn-doped CdS (iii)3% Mn-doped CdS (iv)5% Mn-doped CdS nanoparticles.

Table 2. The results of crystallite size and lattice strain of the Halder Wagner method, Size-strain plot method, Williamson-hall method, Brus Equation size, TEM (ImageJ2 Software) and Debye-Scherrer Size (nm).

Compound	Halder Wagner (D) (nm)	Size Strain Method (D) (nm)	W-H method (D) (nm)	Brus Equation Size (D)(nm)	Strain (Ɛ)	HRTEM Nanoparticles Size (nm)	Debye-Scherer Size (nm)
Pure CdS	3.65	2.95	3.46	3.35	4.03	-	2.29
CdS:Mn(1%)	3.46	2.74	3.49	2.8	4.01	-	2.26
CdS:Mn(3%)	3.16	2.43	3.63	2.74	3.93	2.8914	2.18
CdS:Mn(5%)	2.99	2.03	3.52	2.26	3.99	2.6522	2.16

The first theoretical calculation for semiconductor nanoparticles (using CdS) was provided by the Brus equation and was based on the "effective mass approximation" (EMA). According to this approximation, an exciton is thought to be contained within a sphere-shaped region of the crystallite, and the effective masses ($me=0.13m_o=0.13x9.07x10^{-31}$`and mh=0.45mo=

$0.45x9.07x10^{-31}$`) used to define the wave function are used in place of the electron and hole masses. The first term in Equation (16)'s right-hand side denotes the band gap energy of bulk materials, which is a property of the material. Quantum confinement's extra energy, which is dependent on band gap energy, is represented by the second additive term of the equation. In fact, it can be viewed as the band gap's infinite square-well contribution.

According to the Brus equation, the confinement energy for semiconductor nanocrystals with spherical shapes is inversely proportional to the square of the nanocrystal's radius. The Brus equation is represented by equation (16).

$$E_{g\,(nano)} = E_{(bulk)} + h^2 / 8\, r^2\, (1/m_e + 1/ m_h) - 1.786/ 4\, \pi\, R^2\, \varepsilon_r\, \varepsilon_0 * e^2 \qquad (16)$$

where, $E_{g\ (nano)}$ = band gap energy of nanoparticles, $E_{(bulk)}$ = band gap energy of bulk semiconductor, R = radius of nanoparticles, m_e = effective mass of excited electron, h = Planck's constant, m_h = effective mass of excited hole.

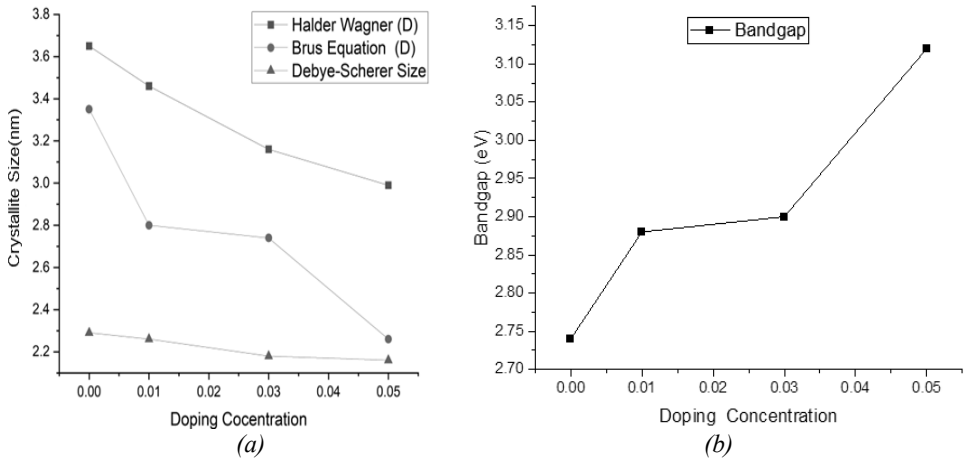

Fig. 9. (a) Plot of Crystallite size vs. doping Concentration (b) Plot of Bandgap vs. doping Concentration.

The crystallite size taken by various methods and band gap variation with an increasing doping concentration of Mn in CdS NPs has been shown in figures 9a and 9b.

3.8. Energy-dispersive X-ray Analysis

X-ray characterization techniques used for defining non-materials include small-angle X-ray scattering, X-ray absorption fine structure (XAFS), X-ray diffraction, and X-ray photoelectron spectroscopy (XPS). The types and quantities of elements at the nonmaterial surface or adjacent to the surface are examined using energy-dispersive X-ray analysis (EDX) in conjunction with scanning electron microscopy (SEM) to generate a sample map (SEM). Electron beams passing through the sample during an EDX analysis produce images of the sample's elements. The specific region images(surface morphology) of Mn-doped CdS nanoparticles are shown in Fig. 10 and the EDX spectra showing the elemental composition of various elements present in the sample are shown in Fig. 11 & Table 3 displays the compositional analysis of the synthesized samples. The outcome of the EDX investigation clearly shows that proportionate amounts of Cd, Mn, and S were present in the samples.

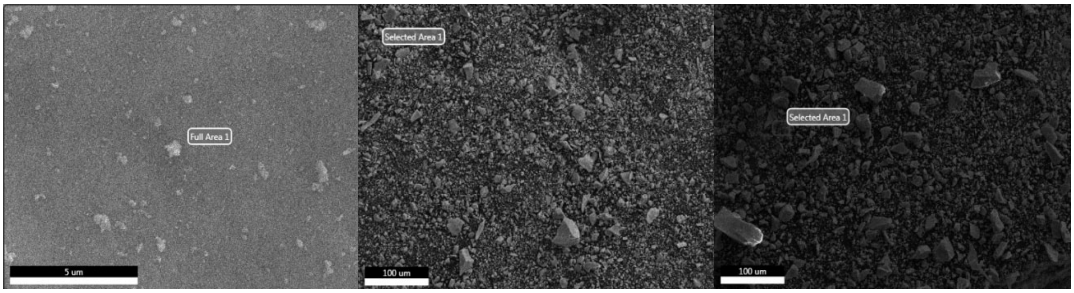

Fig. 10. EDAX of CdS: Mn (1wt%,3wt%,5wt%).

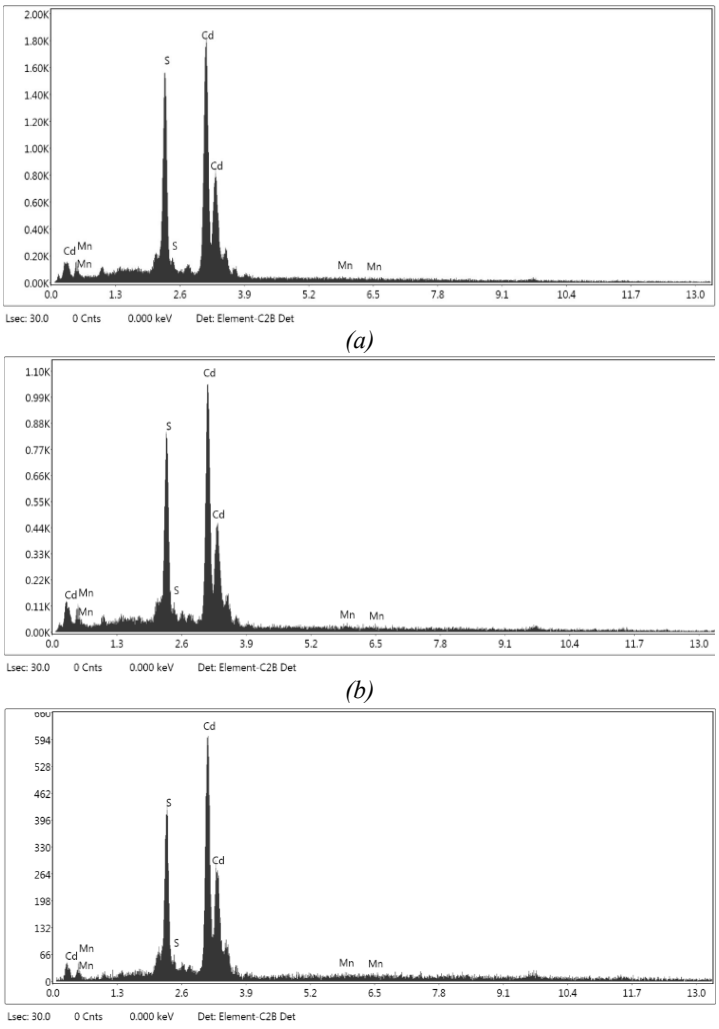

Fig. 11. Energy dispersive x- ray spectra (EDX) of (a)CdS: Mn (1wt%) (b) CdS: Mn (3wt%)(c) CdS: Mn (5wt%).

The EDAX spectra of Mn-doped CdS (1%, 3%, 5%) nanoparticles in Fig. 11 demonstrate that no other pollutants or impurities were present in the samples. It demonstrates unequivocally that as Mn concentrations are added, the strength of Mn peaks grows.

Table 3. -EDX compositional analysis of the prepared samples.

Sample	Element	Weight%	Atomic%	Net Int.	Error %	Kratio
Mn Doped CdS (1%)	S K	23.30	51.36	506.57	4.64	0.2233
	CdL	76.08	47.84	638.64	2.97	0.6718
	MnK	0.62	0.80	4.72	60.04	0.0059
Mn Doped CdS (3%)	S K	20.53	47.16	142.14	5.61	0.1967
	CdL	78.40	51.39	213.06	3.98	0.7034
	MnK	1.08	1.45	2.62	62.50	0.0102
Mn Doped CdS (5%)	S K	22.69	50.11	279.87	4.97	0.2173
	CdL	75.53	47.59	361.11	3.45	0.6689
	MnK	1.79	2.31	7.71	43.29	0.0169

3.9. High-Resolution Transmission Electron Microscopy (HRTEM)

By measuring with TEM, the crystalline structure and quality of each synthesized nanoparticle were evaluated. The size and structure of the generated Mn (3% and 5%) doped CdS nanoparticles were studied using TEM. Figure 12 (a,b) and (c,d) shows the TEM and SAED images of 3% and 5% Mn-doped CdS nanoparticles.

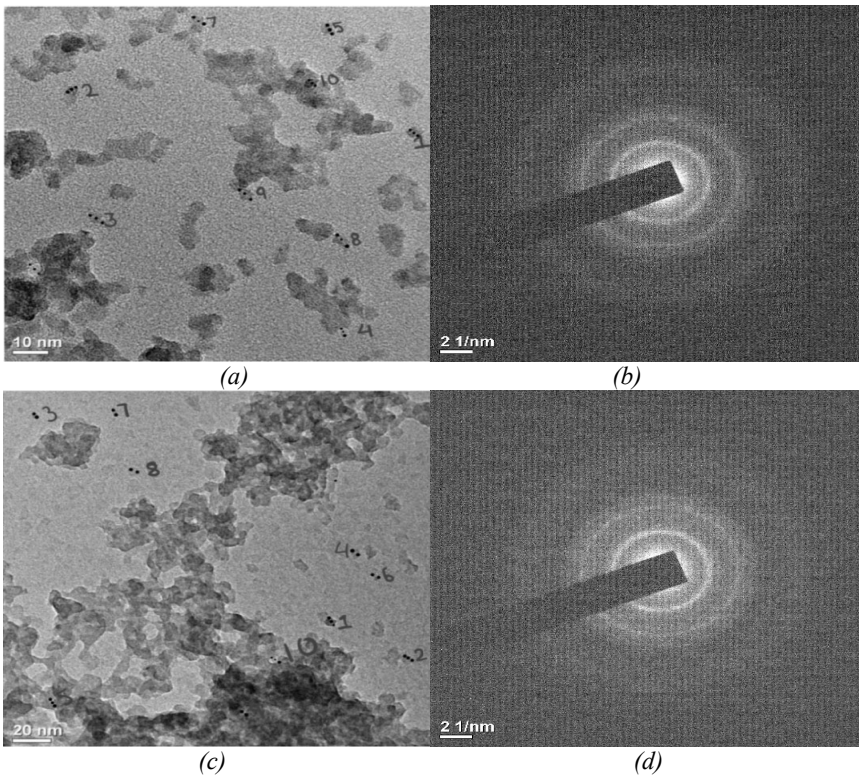

Fig. 12. HRTEM and SAED images of (a,b) Mn (3%) doped CdS nanoparticles (c,d) Mn (5%) doped CdS NPs.

Additionally, ImageJ2 software was used to precisely measure the nanocrystalline size of the sample that was provided. The average size of the 10 nanoparticles in Fig. 12(a), which account for 3% of the sample, is 2.8914 nm, whereas the average size of the samples in Fig. 12 (c), which represent 5% of the sample, is 2.6522 nm and they also have the typical random spherical structure of Mn-doped CdS nanoparticles synthesized through microwave method. The created

nanoparticles have a smooth surface. The image indicates the particles to be abundant, highly distinguishable, and only slightly expanded. The TEM image shows that the sample is spherical and mono-dispersed.

4. Conclusion

Manganese-doped cadmium sulphide semiconductor nanoparticles (CdS: Mn) NPs have been synthesized via microwave-assisted solvothermal technique at different Mn concentrations (0, 1%, 3%, and 5%). The XRD spectra show three major peaks at 2θ equals 26.52°, 44.16°, and 52.32° for pure CdS. The slight changes have been observed in 2θ for 1%, 3%, and 5% doping of Mn in CdS NPs. The peaks correspond to (1 1 1), (2 2 0), and (3 1 1) planes which indicate a cubic structure of the samples. Using FWHM and Debye Scherer equation the size of the nanoparticles was calculated which are 2.29 nm, 2.26 nm, 2.18 nm, and 2.16 nm respectively for pure and Mn (1%, 3%, and 5%) doped CdS.

The reduction in nano-particle size in the Mn-doped CdS sample with increasing concentration may be due to the replacement of Cd^{2+}ion by Mn^{2+}ion. The ionic radii of Mn^{2+} (0.66Å) are smaller than that of Cd^{2+}(0.98 Å), which indicates that the lattice constant decreases when Mn-doped CdS concentration increases. Williamson-Hall, size-strain plot, and Halder-Wagner plots were also introduced in this study to calculate the size and microstrain of the synthesized NPs, and the results were found to be in close agreement as obtained by the Debye Scherrer method. A UV-visible spectrophotometer was used to examine the optical properties of the prepared samples between the wavelength range of 200 to 800 nm. The developed samples Mn (0, 1%, 3%, and 5%) doped CdS have an optical band gap of 2.74 eV, 2.88 eV, 2.90 eV, and 3.12 eV respectively. FTIR spectra from 400 to 4000 cm^{-1}, in the higher energy region, the peak at 3460 cm-1 are assigned to O-H stretching of absorbed water on the surface of CdS. The presence of water is confirmed by its bending vibration at 1550 cm^{-1}.

The size of the generated nanoparticles was studied using HRTEM. It also validates the nanocrystalline structure of the sample. The average size of randomly selected nanoparticles for 3% and 5% Mn-doped CdS is found to be 2.8914 nm and 2.6522 nm.

Acknowledgments

The authors would like to express their deep regards to Prof.(Dr) Arvind Kumar, Director of Birla Institute of Technology, Patna campus for providing all necessary facilities for conducting the experimental work to synthesize nanoparticles. The authors are also thankful to the Central Instrumentation Facility BIT Mesra, Department of Chemistry BIT Patna, IIT Madras, and NEHU Shillong for various characterization work.

References

[1]H K Jun, M A Careem and A KArof, Renew. Sust. Energ. Rev. 22 148(2013); https://doi.org/10.1016/j.rser.2013.01.030

[2]Shweta Chaure, Materials Research Express, 6 2(2018); https://doi.org/10.1088/2053-1591/aad4e1

[3]S. K. Choubey, K. P. Tiwary, Digest Journal of Nanomaterials and Biostructures, 11(1) 33(2016).

[4] Cancan Jin, Kankai Wang, Anthony Oppong-Gyebi, Jiangnan Hu, International Journal of Medical Sciences17(18) 2964(2020); https://doi.org/10.7150/ijms.49801

[5]Nadeem Baig, Irshad Kammakakam, Wail Falath, Mater. Adv.21821(2021).

[6] R. Ranjan, C. M. S. Negi, K. P. Tiwary, Chalcogenide Letters,20(4), 251(2023);

https://doi.org/10.15251/CL.2023.204.251

[7] Tianxing Li, Xiaoping Zou, Hongquan Zhou, International Journal of Photo-energy, ID569763, 6(2014); https://doi.org/10.1155/2014/569763

[8] S. K. Choubey, A. Kaushik, K. P. Tiwary, Chalcogenide Letters, 15(3) 125(2018)

[9] Ibrahim Khana, Khalid Saeed, Idrees Khan Arabian, Journal of Chemistry, 12(7) 908(2019); https://doi.org/10.1016/j.arabjc.2017.05.011

[10] K. P. Tiwary, F. Ali, R. K. Mishra, S. Kumar, K. Sharma, Digest Journal of Nanomaterials and Biostructures,14 (2) 305(2019).

[11] Christine Barglik-Chory, Christian Remenyi, Cristina Dem, Michael Schmitt, et.al PCCP5(8)1639(2003); https://doi.org/10.1039/b300343d

[12] Pratibha R. Nikam, et.al Journal of Alloysand Compounds.689394(2016)

[13] K P Tiwary, F. Ali, R K Mishra, S K Choubey, K Sharma, Journal of Ovonic Research, 16(4) 234(2020).

[14]Jianing Zhao, Xiaoli Li, Zhiguo Li, Journal of Nanomaterials 2015(2015); https://doi.org/10.1155/2015/109734

[15] Nikita H. Patel, M.P. Deshpande, Sandip V. Bhatt, Kamakshi R. Patel, et.al Advanced Materials Letters 5(11):671(2014); https://doi.org/10.5185/amlett.2014.1574

[16] Uma Shankar Patel, Rakesh Kumar Ahirwar, Anjali Bhatt, B. S. Arya, AIP Publishing, 2100(1) 2019; https://doi.org/10.1063/1.5098719

[17]Ruby Chauhan, Ashavani Kumar, Ram Pal Chaudhary, Research on Chemical Intermediates 39 645(2013); https://doi.org/10.1007/s11164-012-0586-x

[18] A. Gadalla, M. Almokhtar, A. N. Abouelkhir, Chalcogenide Letters, 15(4), 207(2018).

[19] Ankit Goyal, Vinay Sharma, Abhishek Sharma, Ravi Agarwal, K.B. Sharma, S.L. Kothari, J. Nano- Electron. Phys.3(1) 254(2011)

[20] Mahmoud Nasrollahzadeh, Zahra Issaabadi, S. Mohammad Sajadi. RCS Advances .83723 (2018).

[21] Anshu Dandia, Vijay Parewa, Kuldeep S. Rathore, Catalysis Communications 28 90(2012); https://doi.org/10.1016/j.catcom.2012.08.020

[22] K P Tiwary, K. Sharma, Neha Bala, Firdaus Ali, Materials Today: Proceedings 18 (3) 1380(2019); https://doi.org/10.1016/j.matpr.2019.06.604

[23] S K Choubey, K P Tiwary, Digest Journal of Nanomaterials and Biostructures 11 (1) 33(2016).

[24] KP Tiwary, F Ali, SK Choubey, RK Mishra, K Sharma, Optik 227 166045(2021); https://doi.org/10.1016/j.ijleo.2020.166045

[25] N. Susha, Rejo Joseph Mathew, Swapna, J Mater Sci, 51(23) (2016); https://doi.org/10.1007/s10853-016-0273-1

[26] Anshu Dandia, Vijay Parewa, Kuldeep S. Rathore, Catalysis Communications, 90(2012); https://doi.org/10.1016/j.catcom.2012.08.020

[27] Kadhim Gbashi, Malek A. H. Muhi, Allaa A. Jabbar, Natheer B. Mahmoodet. al, Applied Physics, 126(8) (2020); https://doi.org/10.1007/s00339-020-03801-1

[28] Bruno Chandrasekar, R. Chandramohan, R. Vijayalakshmi, Journal of Nano-engineering and Nano-manufacturing 3(3) 1(2013); https://doi.org/10.1166/jnan.2013.1141

[29] A. A. Gadalla, A. N. Aboelkhir, M. G. Mahesha, Ashok Rao, Journal of Materials Science: Materials in Electronics, 31,10941(2020); https://doi.org/10.1007/s10854-020-03240-x

[30] K. Pitchaimani, L. Amalraj, S. Muthukumaran, J Mater Sci: Mater Electron, (2016).

[31] SarabSaadi.et.al, NeuroQuantology, 20(1) 199(2022); https://doi.org/10.14704/nq.2022.20.1.NQ22074

[32] Selma M. H. AL-Jawad, Natheer Jamal Imran, Kahlaa H. Aboud, Journal of Sol-Gel Science and Technology,100(5) (2021); https://doi.org/10.1007/s10971-021-05656-1

[33] Nikita H. Patel, M.P. Deshpande, Sandip V. Bhatt, Kamakshi R. Patel, S. H. Chaki, Advanced

materials letters, 5(11), 671(2014); https://doi.org/10.5185/amlett.2014.1574
[34] A. SathiyaPriya, I. B. Shameem Banua, J. Thirumalai, A. Alagar, Optoelectronics and Advanced Materials - Rapid Communications 7(3-4), 191 (2013).